ISSN 1063-7788, Physics of Atomic Nuclei, 2014, Vol. 77, No. 11, pp. 1400–1414. © Pleiades Publishing, Ltd., 2014.
Original Russian Text © Yu.E. Penionzhkevich, 2014, published in Yadernaya Fizika, 2014, Vol. 77, No. 11, pp. 1465–1479.

NUCLEI
Experiment

Radioactive Nuclear Beams: Present and Future

Yu. E. Penionzhkevich*

Joint Institute for Nuclear Research, Dubna, Moscow oblast, 141980 Russia
National Research Nuclear University MEPhI, Dolgoprudnyi, Russia

Received January 13, 2014

Abstract—Some results of investigations into a new nuclear-physics field associated with the production of radioactive nuclear beams and physical studies with these beams are presented. The most recent results obtained by studying the structure of nuclei and reaction mechanisms with radioactive nuclear beams are surveyed. Data obtained in Dubna at the DRIBs accelerator complex are presented along with allied results from other research centers. In this connection, existing experimental data on light loosely bound exotic nuclei are discussed. The parameters of DRIBs3, which is a new accelerator complex, are presented, and the physics research program that will be implemented with the aid of new setups, including a high-resolution magnetic analyzer (MAVR) and a 4π neutron detector (TETRA), is described. A collaboration in the realms of employing radioactive nuclear beams at the DRIBs complex together with other accelerator complexes [SPIRAL2 (France), RIKEN (Japan), FAIR (Germany), and RIBF (США)] on the basis of employing new highly efficient experimental facilities has already led to the discovery of new phenomena in nuclear physics and will make it possible to study in the future new regions of nuclear matter in extreme states.

DOI: 10.1134/S1063778814110052

1. INTRODUCTION

Experimental investigations based on employing radioactive nuclear beams are a new, rapidly developing, line of research in the physics of exotic nuclei. Investigations along this line become broader, which is due to the appearance in many countries worldwide of new powerful intermediate-energy heavy-ion accelerators, including the UNILAC–SIS–ESR accelerator complex and the FAIR accelerator complex under construction in Darmstadt (Germany), the GANIL–SPIRAL1 accelerator complex and the SPIRAL2 complex under construction in Caen for accelerating radioactive beams (France), the heavy-ion accelerator at RIKEN (Japan), a superconductor cyclotron and a new factory of radioactive ion beams (FRIB) under construction in Michigan (USA), the heavy-ion cyclotron complex supplemented with a storage ring and deployed in Lanzhou (China), the superconductor cyclotron in Catania (Italy), and the DRIBs heavy-ion cyclotron complex at the Flerov Laboratory of Nuclear reactions at the Joint Institute for Nuclear Research (JINR, Dubna, Russia). A new generation of accelerators providing high-flux (up to 10^{14} s^{-1}) beams of charged particles from protons and helium nuclei to uranium ions permitted implementing a new stage in studying the properties of exotic nuclei with the aid of radioactive nuclear beams.

Figure 1 gives a roadmap of creation of accelerator complexes for the production of radioactive nuclear beams. This figure shows that, to the end of the period spanning 2015 and 2017, all large research centers worldwide will have developed means for producing such beams. To 2020, it is planned to implement the European project of a factory of radioactive nuclear beams—EURISOL.

This new line of research into nuclear physics has already made it possible to discover a number of interesting phenomena associated with the properties of nuclei remote from the beta-stability valley. At the present time, the average intensity of secondary radioactive nuclear beams is 10^5 to 10^8 s^{-1}. Experiments aimed at studying the interaction of radioactive nuclei with target materials were performed at these intensities, and information about nucleonic radii of nuclei was deduced from an analysis of data obtained in those experiments. An anomalously large radius of the neutron distribution (neutron halo) in the ^{11}Li nucleus was found, and searches for a neutron halo in neutron-rich nuclei, including ^{6}He, ^{8}He, and ^{14}Be, as well as for a proton halo (an anomalously large radius of the proton distribution) in neutron-deficient nuclei, including ^{8}B and ^{17}Ne, are being performed.

*E-mail: pyuer@jinr.ru

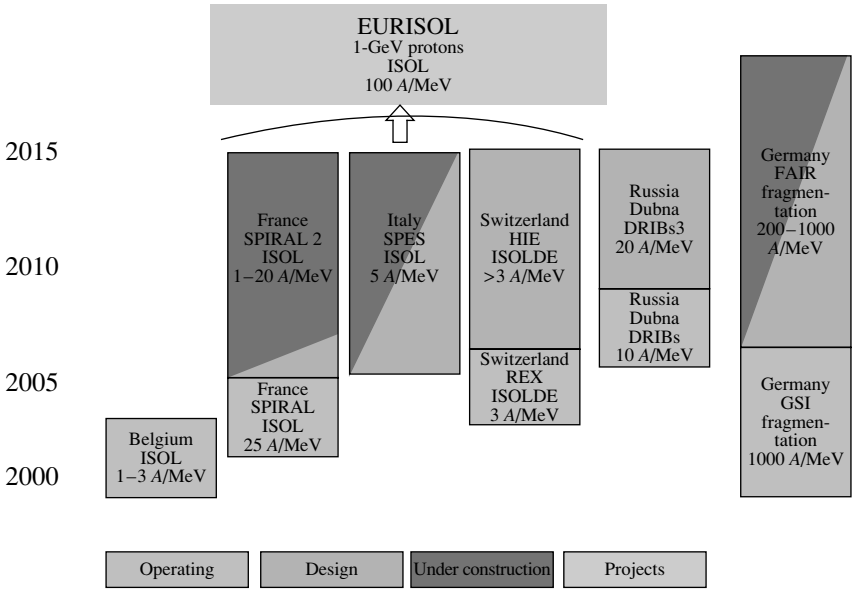

Fig. 1. Roadmap of the Nuclear Physics European Community (NUPEC) for the implementation of projects of accelerator complexes for the production of radioactive nuclear beams.

2. METHODS FOR OBTAINING RADIOACTIVE NUCLEAR BEAMS

The use of radioactive nuclear beams in physics studies involves three problems: (i) the production of beams themselves that would have the required intensity, (ii) their acceleration to the required energy, and (iii) the detection of products of nuclear reactions induced by radioactive nuclei.

There are two basic methods for the production of radioactive nuclei in reactions involving charged particles. The first consists in employing heavy-ion beams that, after undergoing acceleration to an energy in excess of 30 MeV per nucleon, bombard targets. In that case, the bombarding ions undergo fragmentation leading to the formation of nuclear-reaction products that have broad charge and mass distributions and a narrow forward-oriented angular distribution, their velocities being commensurate with the primary-beam velocity. After selecting the required nuclei in Z and A with the aid of magnetic fragment separators, one can employ the emerging radioactive nuclear beams without subsequently accelerating them. Within the second method, protons or heavy ions of energy up to 30 MeV per nucleon are first accelerated to an energy of several GeV units per nucleon and are then directed to a thick target, where the energy of bombarding particles is entirely absorbed. In that case, the fragmentation of target nuclei under the effect of high-flux beams leads to the formation of radioactive nuclear-reaction products that have broad distributions of Z and A and which remain in the target material. For a further employment of these nuclei, it is necessary to extract them from the target and to accelerate them to the required energy. This is accomplished by applying special mass separators supplemented with a system for the transportation of the ions and their subsequent acceleration.

The possibility of obtaining beams of short-lived nuclei (whose lifetime does not exceed a few microseconds) is an advantage of the first method, but, because of limitations on the target thickness (about 500 mg cm^{-2}), the yield of radioactive nuclei is not as high as in the case of full ion absorption in the target. The second method is usually used to obtain intense radioactive beams of nuclei that have a relatively long lifetime ($\tau_{1/2} > 0.5$ s). The limitation on the lifetime of such nuclei is explained by the time of their diffusion from the target.

There is a project where radioactive nuclear beams originate from a high-flux nuclear reactor. Upon irradiating a ^{235}U target with a thermal-neutron flux in the core of such a reactor, one can obtain a high yield of fragments whose mass number A ranges between 80 and 100.

Yet another method for producing high-intensity radioactive nuclear beams is based on photofission reactions in which use is made of a photon flux obtained at high-flux electron accelerators of energy 50 MeV. Within a special converter, an electron beam is transformed into photons. Transporting thereupon radioactive beams of fission fragments to a source of multiply charged ions and accelerating them at a cyclotron, one can obtain radioactive nuclear beams of intensity up to 10^{10} s^{-1} in the fission-fragment

mass range if the total efficiency of the whole system is about 10^{-4} [1, 2].

The intensity of secondary beams can be represented in the form

$$I_{\text{sec}} = I_{\text{pri}} \frac{N_{\text{A}}}{M} \sigma d \varepsilon_{\text{esc}} \varepsilon_{\text{trans}} \varepsilon_{\text{ion}} \varepsilon_{\text{acc}}, \qquad (1)$$

where σ is the total reaction cross section in cm^2 units, d is the target thickness in g cm^{-3} units, M is the mass number of the target element, N_{A} is Avogadro's number, and ε stands for the efficiency of respective processes from the escape of a nucleus from the target (ε_{esc}) to its withdrawal from a postaccelerator (ε_{acc}). In considering various methods for the production of radioactive nuclear beams, it is therefore necessary to take into account all of these factors, which affect the maximum beam intensity.

The intensity of some radioactive nuclear beams may be as high as 10^9 s^{-1}. Such beams came to be used in experimentally studying the properties of exotic nuclei [3].

3. INVESTIGATIONS WITH RADIOACTIVE NUCLEAR BEAMS

Accelerated radioactive nuclear beams provide the possibility of producing and studying nuclei featuring the maximum possible number of neutrons (neutron-rich nuclei) or protons (proton-rich nuclei). This permits making substantial advancements along traditional lines in nuclear physics: synthesis of new nuclei and investigation of their properties, which, as even the first experiments with radioactive beams showed, may differ substantially from the properties known or predicted earlier for nuclei in the stability valley. Radically new information about nuclear-reaction mechanisms, which may be substantially affected by the structure of interacting nuclei, can be obtained by using such beams. Radioactive beams are efficiently used in astrophysics and applied studies. Some results obtained by studying the structure of exotic nuclei with the aid of radioactive nuclear beams are presented below.

3.1. Masses and Binding Energies

A determinations of binding energies and masses of nuclei is one of the fundamental problems in nuclear physics. In nuclear physics, the mass is one of the fundamental quantities that serves as a basis for constructing and testing various nuclear models. An analysis of possibilities for measuring nuclear masses and employing them in nuclear physics was given in [4].

In recent years, this problem has successfully been solved with the aid of radioactive nuclear beams. After the advent of beams of radioactive nuclei, it became possible to measure their mass precisely (to a precision of $\Delta M/M \approx 10^{-6}$). For this, use is usually made of time-of-flight systems featuring a rather long flight base ($L \approx 2$–3 km). In that case, the mass resolution is given by

$$\Delta M/M = 2[\Delta T/T + \Delta L/L] + \Delta E/E, \qquad (2)$$

where T is the flight time.

A large series of mass measurements for light nuclei was performed at the GANIL accelerator complex (France) by using a special magnetic spectrometer whose flight base is 82 m. Radioactive nuclei from ^{27}F to ^{46}Cl were studied in those experiments, and their masses were determined [5]. Considerable advances in precisely measuring masses (to a precision as high as 10^{-8}) have been made after the advent of storage rings for beams of exotic nuclei. Such nuclei produced in fragment separators are injected into such rings. For example, the masses of about 300 nuclei in the vicinity of the nucleon drip line have been measured in recent years at GSI (Darmstadt) by using the SIS–FRS–ESR storage ring featuring electron cooling.

The binding energy as a function of the number of neutrons has the shape of a rather smooth curve showing deviations near closed shells in view of an increase in the neutron binding energy S_n for magic nuclei.

Figure 2 shows the dependences of the separation energy for one neutron and of the energy of the 2^+ level on the number of neutrons in nuclei. In these dependences, one can see manifestations of the $N = 20$ and $N = 28$ shells for silver, calcium, and titanium isotopes. However, the values measured for the energy of the 2^+ level in ^{32}Mg [$E(2^+) = 885.5(7)$ keV, while $E(4^+) = 1430(3)$ keV] and ^{44}S [$E(2^+) = 1297(18)$ keV] nuclei [6] are indicative of a strong deformation of these nuclei. The discovery in the ^{43}S nucleus of an isomeric state characterized by the transition energy of $E = 319$ keV and a lifetime of $T_{1/2} = 488 \pm 48$ ns [7] showed that, in this nucleus, there may coexist two shapes—namely, a spherical shape and a deformed one, which was first predicted by Lutostanskii for ^{31}Na [8].

Anomalous values of the mass and half-life were also obtained for ^{31}Na [9]. The ^{31}Na nucleus, which lies far from the stability valley, proved to have a binding energy higher than that which was expected. Later on, a similar situation was also observed for magnesium isotopes ($^{31-33}$Mg).

A violation of the usual order of population of neutron subshells was hypothesized in order to explain the properties of nuclei in the mass-number range of

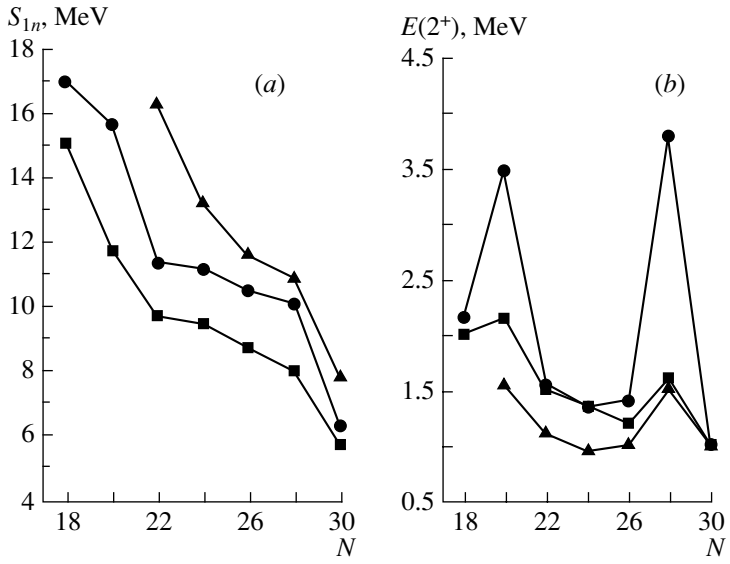

Fig. 2. Dependence of the (*a*) one-neutron separation energy S_n and (*b*) energy of the 2^+ level on N for (closed boxes) argon, (closed circles) calcium, and (closed triangles) titanium isotopes.

28–50. Specifically, it was assumed that neutrons do not populate low-lying *sd* orbitals, leaving a free hole state, but go over to higher lying *pf* orbitals, where they form a filled state. As a result, the nucleus becomes deformed. Such states are referred to as intruder states. The region of nuclei where such effects are manifested is called the inversion region.

Along with S_n, the energy of separation of the last two neutrons, S_{2n}, determines the neutron binding energy in exotic nuclei and has the form

$$S_{2n}(A,Z) = [\Delta\mathrm{M}(A-2,Z) - \Delta M(A,Z) + 2\Delta M_n] \times c^2, \quad (3)$$

where $\Delta M(A,Z)$ is the mass excess for the ${}_ZX^A$ nucleus and ΔM_n is the neutron mass excess, which is equal to 8.071 MeV.

Figure 3 shows the experimental dependence of S_{2n} on the number of neutrons [10]. It can be seen that the binding energy of the calcium, potassium, and argon isotopes is affected by the $N = 20$ and 28 closed shells. For the magnesium, sulfur, phosphorus, silicon, and chlorine isotopes, however, an increase in S_{2n} is observed in the regions around $N = 22$ and $N = 26$. Manifestations of the disappearance of the $N = 28$ shell and the appearance of $N = 26$ shell are especially pronounced for chlorine isotopes. The S_{2n} values measured experimentally [10] for the isotopes ^{41}Si, ^{43}P, and ^{44}S are substantially lower than the values extrapolated on the basis of the mass tables (see Table 1).

This fact is also indicative of the weakening of the effect of closed shells. For the chlorine, sulfur, and phosphorus isotopes, an increase in the neutron binding energy in relation to the calcium, sodium, and argon isotopes in the regions around the numbers of $N = 20$ and $N = 26$ is observed, which can be explained by the deformation creating more strongly bound configurations for these nuclei. Yet another shell, which is formed by $N = 34$ neutrons (^{54}Ca), was recently observed.

Thus, we have seen that, for neutron-rich nuclei, new deformation regions arise near the numbers of neutrons equal to $N = 22$ and $N = 26$, and these regions determine the stability of these nuclei.

The assumption that there exist new closed shells relies on data from experiments devoted to measurements of nuclear masses. In that case, a comparison of the experimental mass excess with the results of the calculations based on the finite-range liquid-drop model (FRLDM) makes it possible to obtain the experimental shell correction dM_{expt} as a function of the number of neutrons in nuclei. Figure 4 gives such dependences for the calcium, sulfur, and phosphorus isotopes between the $N = 20$ and $N = 28$ shells [11]. In the dependence of the mass excess for the calcium isotopes in this figure, there are two minima around

Table 1. Experimental and extrapolated binding energies of two neutrons (S_{2n}) for the ^{41}Si, ^{43}P, and ^{44}S nuclei

Nucleus	S_{2n}^{exp}, keV	S_{2n}^{extr}, keV
^{41}Si	4510 (1870)	6450 (720)
^{43}P	5680 (850)	8220 (690)
^{44}S	7610 (420)	9780 (600)

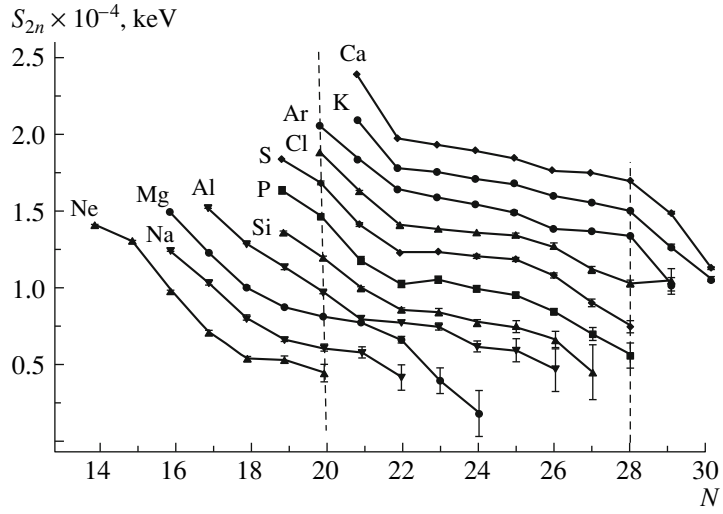

Fig. 3. Separation energy S_{2n} for the last two neutrons as a function of N for neutron-rich nuclei from neon to calcium around the $N = 20$ and $N = 28$ closed shells (vertical dashed lines) [10].

$N = 20$ and $N = 28$. Between these two magic numbers, the change in the binding energy is determined by the filling of the $f_{7/2}$ shell. For the sulfur and phosphorus isotopes, a break in this dependence is observed at $N = 26$. The conclusion that a new shell corresponding to $N = 26$ appears was drawn on this basis. The energy difference between the experimental and extrapolated mass values for the isotopes ^{43}P and ^{44}S was 2.15 and 1.76 MeV, respectively. There are also similar trends for other nuclei, and this leads to the new magic numbers of $N = 6$, 16, and 34 for neutron-rich nuclei instead of $N = 8$, 20, and 40 for nuclei in the stability valley. For example, the number of $N = 6$ instead of the magic number of $N=$ 8 appears for light neutron-rich p-shell nuclei. As a consequence, the ^{8}He nucleus has a sufficient binding energy, while the isotopes ^{9,10}He are unbound. The identical situation prevails for the bound magic nucleus of ^{24}O and unbound $^{25-28}$O. From the point of view of manifestations of new shells, $Z > 8$ neutron-rich nuclei are of interest. As was established experimentally, the neutron drip line is reached at a much greater value of $(N - Z)/Z$ for fluorine, neon, and sodium isotopes than for oxygen isotopes (the last bound isotope of oxygen is ^{24}O). It is interesting that the addition of one proton to the ^{24}O nucleus makes it possible to bind six extra neutrons in the fluorine nucleus (22 neutrons in ^{31}F versus 16 neutrons in ^{24}O). It was also found experimentally that the doubly magic nucleus of ^{28}O ($N = 20$) is unbound. All of this is also indicative of the change in the magic numbers of 8, 20, and 40 for nuclei lying far from the stability valley. It should be emphasized that all these results were obtained with radioactive nuclear beams.

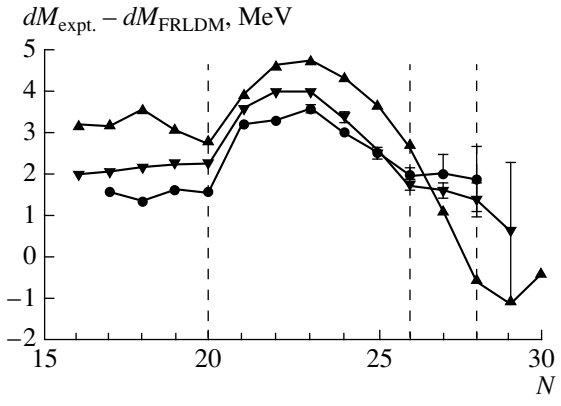

Fig. 4. Deviation of the experimental shell correction dM_{expt} [11] from its theoretical counterpart dM_{FRLDEM} for the (closed inverted triangles) calcium, (closed triangles) sulfur, and (closed circles) phosphorus isotopes around $N = 20$, 26, and 28.

3.2. Spectroscopy of Radioactive Nuclear Beams

Important information about the properties of exotic nuclei was recently obtained by gamma-spectroscopy methods in studying their decay from excited states by using the Coulomb excitation of these nuclei.

The discovery of mixing of $(sd + pf)$ configurations for nuclei featuring a large neutron excess was one of these results. This mixing leads to the superposition of single-particle levels. In that case, the change in the properties of the $N = 20$, $Z \leqslant 12$ isotones is explained not only by valence protons in the sd shell but also by particle–hole configurations

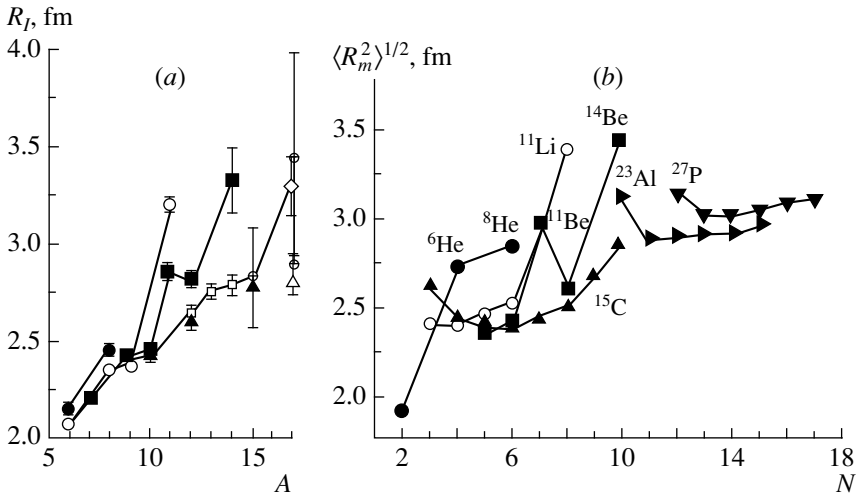

Fig. 5. (a) Interaction ranges R_I extracted for neutron-rich isotopes of light nuclei from the experimental values of the interaction cross sections versus A and (b) their matter radii $\langle R_m^2 \rangle^{1/2}$ versus N: (closed circles) He, (open circles) Li, (closed boxes) Be, (open boxes) B, (closed triangles) C, (cross in the circle) N, (open triangles) F, (diamonds) Ne, (right-oriented closed triangles) Al, and (inverted closed triangles) P.

formed owing to the transition of neutrons from the sd to the pf shell.

The structure of neutron-rich nuclei depends substantially on their isospin. This situation is exemplified by the ^{32}Mg and ^{44}S nuclei, for which it is found that their levels are spaced rather closely, so that the characteristically wide energy gaps between different levels are not observed. It was also found that, in the ^{32}Mg nucleus, the energy of the first excited state is as low as 885 keV, which is much less than values characteristic of "normal" magic nuclei, such as ^{36}S and ^{40}Ca, in which the first excited state lies at an energy of about 3 MeV. This phenomenon was called collective quadrupole excitation and will be discussed below. The potential of experiments with radioactive nuclear beams primarily permits studying 2^+ states and evaluate the reduced probability $B(E2)$.

Using as an example the properties of the isotopes ^{32}Mg and ^{34}Mg obtained as secondary radioactive beams, we can state that, in magnesium isotopes, the deformation grows with increasing neutron excess. From this point of view, the improvement of stability for the doubly magic nucleus ^{40}Mg as for a deformed nucleus can be expected even under the condition of destruction of the $N = 28$ magic shell, and this was confirmed experimentally in [12]. The result in question confirmed compellingly the conclusion that deformation affects the stability of nuclei at the boundaries of the stability valley.

3.3. Nucleon-Density Distribution in Exotic Nuclei

A vast body of information in experiments with beams of light radioactive nuclei was obtained in measuring the radii of these nuclei and nucleon-density distributions in them. In one of the first experiments with beams of lithium isotopes, the interaction cross section (σ_I) was measured as the difference of the total reaction cross section (σ_R) and the elastic-interaction cross section (σ_E): $\sigma_I = \sigma_R - \sigma_E$ [13]. It was assumed that the interaction cross section is equal to the reaction cross section, $\sigma_I = \sigma_R$, and the interaction radius R_I was determined from the relation $\sigma_I = \pi[R_I(P)^2 + R_I(T)^2]$, where P and T are the projectile and target, respectively. The value of $R_I(P)$ is virtually independent of the target mass. Therefore, $R_I(P)$ is a parameter that determines the size of the projectile particle. Subsequent calculations, performed on the basis of the Glauber model, confirmed that the difference of the reaction and interaction cross sections, especially at high energies, does not exceed a few percent. The radii determined in this way for light nuclei from hydrogen to neon are given in Fig. 5. It can be seen that, for stable nuclei, the interaction radius as a function of the nuclear mass is described by the function $R_I \sim A^{1/3}$. For unstable nuclei, however, the radii may differ substantially from the value determined by the standard nuclear-mass increment.

Information about the distribution of protons and neutrons in exotic nuclei is also obtained from data on their elastic scattering off target nuclei. Elastic scattering is usually analyzed on the basis of the optical model and the coupled-channel method, where the real and imaginary parts of the optical potential used are calculated microscopically.

The total M3Y interaction, involving the direct and exchange components of the potential, was used

in [14] to analyze the elastic scattering of exotic nuclei. In that case, the interaction potential is represented in the form of the sum $U(R) = U^D(R) + U^E(R)$, where $U^D(R)$ is the direct potential based on the double-folding model. The second term receives contributions from effects of one-nucleon exchange, These effects can be described within the density-matrix formalism. In constructing the exchange potentials, use is made of the iteration method. The number of iterations depends on energy, mass numbers of colliding nuclei, and the distance R between them. The nucleon-density distributions for projectile and target nuclei are calculated on the basis of the density-functional method with a single parameter set. In that case, the total potential is taken in the form

$$U_i(R) = U(R) + i\left[N_W U(R) - \alpha R\frac{dU(R)}{dR}\right], \quad (4)$$

where $U(R)$ includes a direct and an exchange part, while the imaginary part involves two parameters, N_W and α. This representation of the absorption potential makes it possible to avoid the introduction of a phenomenological imaginary part—for example, in the form of the Woods–Saxon potential. This approach is successfully used to obtain information about the root-mean-square radii of the neutron- and proton-density distributions in nuclei. Table 2 [15] lists the radii obtained within this approach for various nuclei. Figure 6 shows the neutron- and proton-density distributions in the same nuclei. The tail of the neutron distribution in the ^{11}Li is well-pronounced. One can also see that, on the side of the proton drip line, the tails of the proton densities in ^{8}B and ^{7}Be exceed substantially the neutron tails, and this give grounds to state that a proton skin exists in these two nuclei.

Nuclei at the nucleon drip line has an extremely low binding energy of valence nucleons. For example, the neutron binding energy in stable nuclei is 6 to 8 MeV, but, in highly neutron-rich nuclei, such as ^{11}Li, ^{11}Be, and ^{14}Be, the binding energy of a neutron (or two neutrons) is as low as a few hundred keV units. This leads to a very broad neutron-density distribution in such nuclei (see Fig. 6).

3.4. Momentum Distribution of Loosely Bound Nuclei

Measurement of the momentum distribution of products originating from the fragmentation of halo nuclei (that is, the core and halo neutrons) is one the methods for obtaining information about the neutron halo—in particular, about correlations between halo neutrons.

Almost all nuclei that have a two-neutron halo are stable against nucleon emission, while nuclei differing from them by one neutron are unstable against nucleon emission. It is common practice to refer to nuclei featuring a two-neutron halo as Borromean nuclei. Thus, correlations between two valence nucleons stabilize halo nuclei.

The momentum distribution of a neutron in the breakup of a nucleus is determined by the Fourier transform of its harmonic-oscillator wave function and is written in the form of a Gaussian function as

$$f(p) = C/(p_i^2 + k^2). \quad (5)$$

The width of the momentum distribution depends on the parameter k. In contrast to what we have for the matter-density distribution, a decrease in E_n leads to a decrease in the width of the momentum distribution. This is an obvious consequence of the uncertainty principle: if the spatial distribution is broad, the momentum distribution is narrow. Thus, the presence of a neutron halo in nuclei determines an extended spatial neutron-density distribution, to which a narrow momentum distribution of their decay product corresponds.

In the fragmentation model proposed by Goldhaber [15], the width of the momentum distribution of fragments is described in terms of Fermi motion or temperature corresponding to the binding energy. This model makes it possible to obtain an expression for the width of the momentum distribution of a bombarding-ion fragment as a function of the mean separation energy for outer valence nucleons ($\langle\varepsilon\rangle$), the fragment mass ($A_F$), and the projectile mass (A_P). Specifically, we have

$$\sigma^2 = 2u\,\langle\varepsilon\rangle\,\frac{A_F(A_P - A_F)}{A_P}, \quad (6)$$

where u is an atomic-mass unit, or

$$\sigma^2 = 2u\,\langle\varepsilon\rangle\,\frac{A_P - 1}{A_P} \quad (7)$$

for the separation of one nucleon.

The longitudinal-momentum distribution of the core nucleus reflects directly the wave function for the ground state of a halo nucleus—that is, the intrinsic-momentum distribution of halo nucleons.

Measurements of the momentum distributions of fragments produced in the fragmentation of ^{11}Li, ^{11}Be, and ^{14}Be nuclei on various targets (Be, C, Nb, and Ta) were reported in [16, 17]. The results for ^{11}Li and ^{11}Be projectile nuclei are shown in Fig. 7. One can see that the longitudinal-momentum distributions of ^{9}Li nuclei appearing as fragments produced upon ^{11}Li breakup on Be, Nb, and Ta target nuclei are very narrow (see Figs. 7*a*, 7*b*, and 7*c*). The

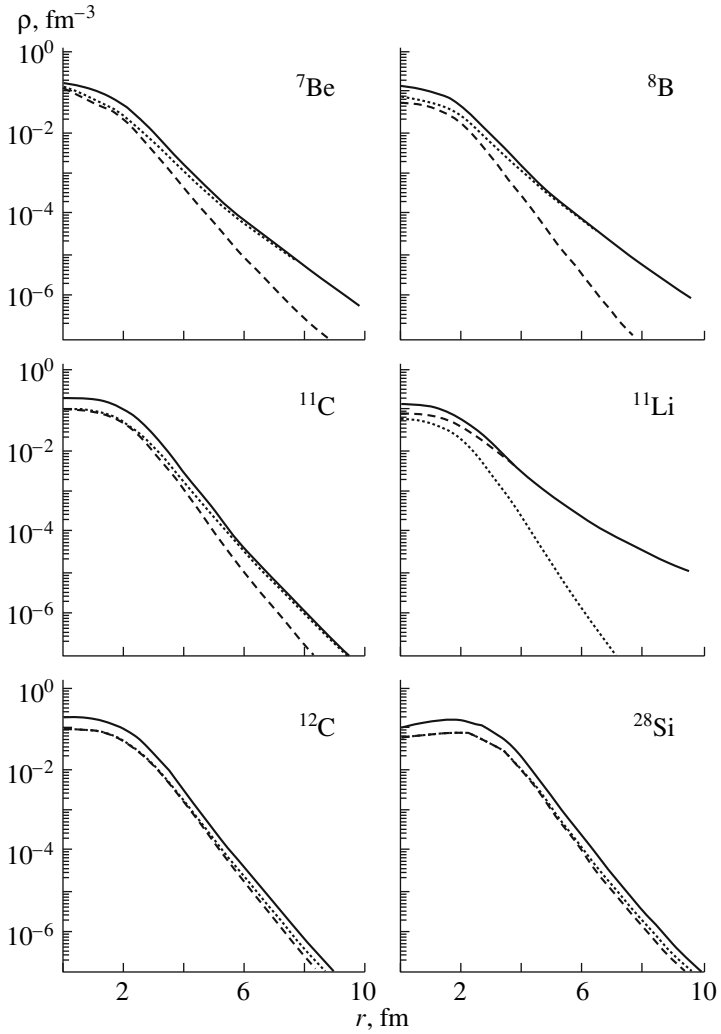

Fig. 6. Distributions of (dashed curve) neutron, (dotted curve) proton, and (solid curve) nuclear-matter densities in various nuclei [15].

transverse-momentum distributions of ^{9}Li and ^{10}Be produced upon ^{11}Li and ^{11}Be breakup on a carbon target feature a narrow component superimposed on a broad distribution (see Figs. 7*d* and 7*e*). In accordance with the uncertainty principle, these small widths of about 20 to 30 MeV/c give sufficient grounds to conclude that halo neutrons features a broad spatial distribution.

Table 2. Root-mean-square radii of the neutron-density distribution ($\langle R_n^2\rangle^{1/2}$) and the proton-density distribution ($\langle R_p^2\rangle^{1/2}$) and root-mean-square matter radii ($\langle R_m^2\rangle^{1/2}$) for various nuclei [15]

Nucleus	$\langle R_n^2\rangle^{1/2}$, fm	$\langle R_p^2\rangle^{1/2}$, fm	$\langle R_m^2\rangle^{1/2}$, fm	δR_{np}, fm
^{7}Be	2.237	2.549	2.420	−0.312
^{8}B	2.190	2.680	2.507	−0.490
^{11}Li	3.255	2.235	3.011	1.020
^{11}C	2.326	2.456	2.398	−0.130
^{12}C	2.387	2.406	2.396	−0.019
^{28}Si	2.953	2.982	2.967	−0.029

Measurements of the momentum distributions of ^{4}He nuclei originating from ^{6}He breakup (at $E \sim$ 10 MeV per nucleon) were reported in [18]. The results of those measurements are presented in Fig. 8. The experimental distributions were approximated by Gaussian functions. Narrow momentum distributions ($\sigma = 28$–29 MeV/c) were observed. If the ^{6}He nucleus were an ordinary nucleus—not a halo-like one—then this quantity would have been about 100 MeV/c. A small width of the momentum distribution confirms the presence of a halo in ^{6}He.

These results were compared with data obtained for ^{4}He nuclei from the breakup of ^{6}Li nuclei (see

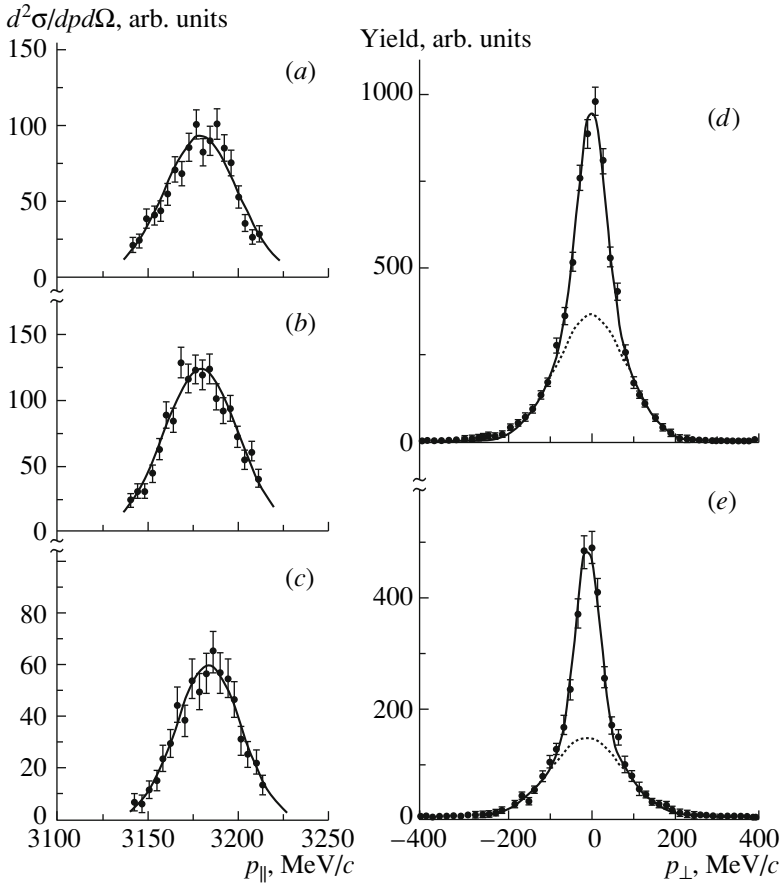

Fig. 7. Experimental longitudinal-momentum distributions of ^{9}Li nuclei produced in ^{11}Li fragmentation on (*a*) Be, (*b*) Nb, and (*c*) Ta targets and transverse-momentum distributions of (*d*) ^{9}Li and (*e*) ^{10}Be nuclei produced in, respectively, ^{11}Li and ^{11}Be fragmentation on a carbon target [16, 17]. The curves represent the results of fitting Gaussian curves of width σ to these distributions for (dotted curves) a wide distribution (σ_{wid}) and (solid curves) the total distribution with allowance for a narrow distribution (σ_{th}). The resulting values of the parameter σ are the following: (*a*) $\sigma_{\text{th}} = 20.9(0.8)$ MeV/c, (*b*) $\sigma_{\text{th}} = 21.2(0.7)$ MeV/c, (*c*) $\sigma_{\text{th}} = 18.7(0.8)$ MeV/c, (*d*) $\sigma_{\text{th}} = 21.3 \pm 3$ MeV/c and $\sigma_{\text{wid}} = 80 \pm 4$ MeV/c, and (*e*) $\sigma_{\text{th}} = 25.4 \pm 4$ MeV/c and $\sigma_{\text{wid}} = 109 \pm 7$ MeV/c.

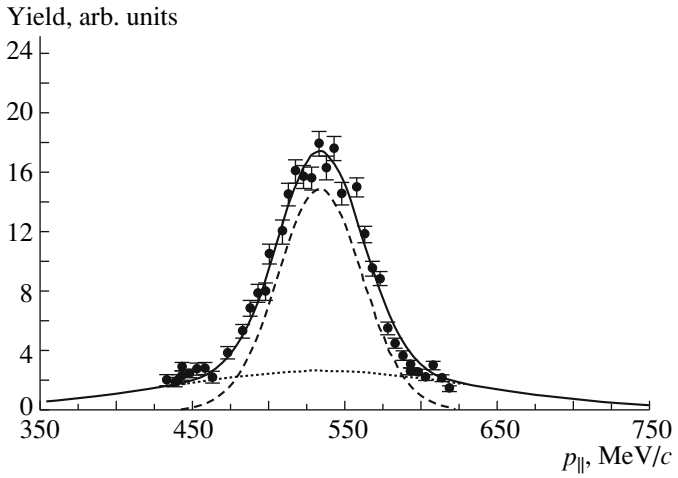

Fig. 8. Momentum distribution of ^{4}He nuclei produced upon ^{6}He breakup on gold nuclei at the energy of 10 MeV per nucleon. The displayed points stand for experimental data. The dashed curve corresponds to the width of $\sigma_{\text{th}} = 28 \pm 1$ MeV/c, while the dotted curve corresponds to the width of $\sigma_{\text{wid}} = 100$ MeV/c. The solid curve represents the sum of the contributions from the two components in question [18].

Fig. 9). The widths of the measured distributions were 46 to 55 MeV/c, and these values are intermediate between the widths of the distributions for ^{6}He breakup and the widths of the distributions for the breakup of ordinary nuclei and are only slightly dependent on the beam energy. The ^{6}Li nucleus is not strongly bound—the threshold for its breakup to an alpha particle and a deuteron is 1.474 MeV [19]. We cannot rule out the possibility that this breakup proceeds from a higher lying state (0^+ , 3.563 MeV), which is an isobar analog of the ^{6}He ground state and which lies below the threshold for the three-body breakup process $^6\mathrm{Li} \to \alpha + p + n$ (3.699 MeV) by a value as low as 136 keV. Therefore, we can explain values in the range of $\sigma \sim 46$–55 MeV/c under the assumption that the excited state of ^{6}Li in question has a halo structure formed by a neutron and a proton outside the alpha particle and characterized by an increase in the radius of the nucleus in this state.

A systematics of the widths σ of momentum distributions of fragments originating from the breakup of various nuclei versus the binding energy of one or two neutrons in these nuclei (see Fig. 9) is presented in [18].

One can see that the width σ grows smoothly with increasing binding energy. In the case of ^{6}Li, the value of σ is presented for the ($^6\mathrm{Li} \to ^4\mathrm{He} + d$) threshold (open circle), as well as for the ($^6\mathrm{Li} \to ^4\mathrm{He} + n + p$) threshold (star). In the last case, the value of σ complies with the trend toward the growth of σ for the remaining nuclei. Thus, there are reasons to believe that this result supports the hypothesis of the existence of an excited state of ^{6}Li in the form of a (np) halo. This state was earlier predicted in [19] and was experimentally supported in [18].

Experimental data on the widths of momentum distributions make it possible to obtain information about the energy of stripping of valence neutrons off exotic nuclei.

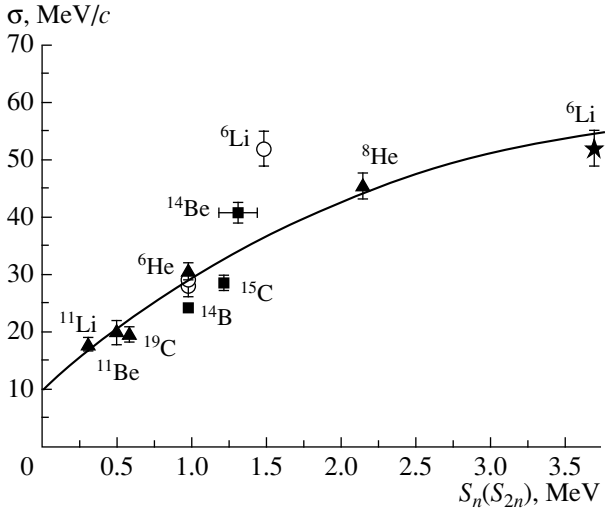

Fig. 9. Systematics of the widths σ of momentum distributions of fragments originating from the breakup of various loosely bound nuclei versus the binding energy of one or two neutrons. Two values for ^{6}Li correspond to the breakup processes (open circle) $^4\mathrm{He} + d$ and (star) $^4\mathrm{He} + n + p$ ($\star$) [18]; the closed boxes and closed triangles stand for, respectively, data from the literature and averaged data from the literature . The solid curve represents the results of fitting a polynomial of third degree to the data.

4. REACTIONS INVOLVING EXOTIC NUCLEI

4.1. Elastic Scattering of Exotic Nuclei

An analysis of the angular distributions for the elastic scattering of nuclei furnishes information about the shape and magnitude of the nuclear potential, as well as about the parameters of the nuclei themselves (their shapes, root-mean-square radii of nucleon and charge distributions, etc.). As a rule, use is made of various approaches to analyzing angular distributions of elastically scattered nuclei, including the semiclassical approach and phenomenological or semimicroscopic optical models. In accordance with a semiclassical treatment of elastic scattering, a particle moves along a classical trajectory and may undergo inelastic interaction pushing it outside the elastic channel. Studying the dependences of elastic-scattering experimental data on the closest approach distance

$$D = a/2\left(1 + \mathrm{cosec}\,\frac{\theta}{2}\right), \quad a = \frac{2}{E} Z_p Z_t e,$$

where Z_p and Z_t are, respectively, the projectile and target charge numbers, E is the projectile energy, and θ is the scattering angle, one can then determine both the particle-interaction range and the strong-absorption radius—that is, the distance between the centers of colliding nuclei at which the flux intensity in the elastic channel decreases by a factor of two. Experiments performed in beams of ^{6}He, ^{9}Li, and ^{11}Li radioactive nuclei and aimed at studying their elastic scattering were reported in [20]. A strong difference in the angular distributions between ^{6}He and ^{6}Li nuclei, as well as between ^{7}Li and ^{11}Li nuclei, was found in those experiments. An analysis of this difference revealed that it may be due to the effect of the neutron halo in the ^{6}He and ^{11}Li nuclei. Thus, the existence of a neutron halo in some nuclei was confirmed in experiments that studied elastic scattering of radioactive nuclei. Experiments to study the elastic scattering of a beam of ^{8}B nuclei revealed that, in this nucleus, the proton distribution is wide, having a radius larger

than the radius of the neutron-density distribution (proton halo).

A series of experiments devoted to studying the elastic scattering of ^{6}He nuclei on various targets, including a hydrogen target, was performed at the Laboratory of Nuclear Reactions at the Joint Institute for Nuclear Research (JINR, Dubna, Russia). An analysis of data obtained in those experiments led to the conclusion that there is a dineutron configuration in ^{6}He [21]. Experiments along this line of research are quite promising from the point of view of obtaining information about potentials of exotic nuclei, but they require vast statistics, especially in the region of backward angles, and, hence, high intensities of radioactive nuclear beams. These are experiments for the future.

4.2. Complete-Fusion Reactions

For nearly ten years, the problem of interaction of nuclei featuring a neutron halo has been a subject of experimental and theoretical studies. However, the problem of special features of interaction of such nuclei has yet to be clarified conclusively. Of particular interest from this point of view are reactions that are induced by beams of ^{6}He nuclei and in which the formation of compound nuclei is followed by their decay through the neutron-evaporation or fission channels. The first experimental study devoted to the fission of the ^{215}At compound nucleus produced in the interaction of ^{6}He with ^{209}Bi nuclei was reported in [22], and a substantial growth of the cross section in the subbarrier energy region in relation to the results of the calculations based on the statistical model was found there. Somewhat earlier, the effect of enhancement of the fusion probability was predicted in a number of theoretical studies [23]. Among other things, it was shown for ^{11}Li that the probability of penetration (tunnelling) through the potential barrier may increase owing to a more extended distribution of the neutron density in it in relation to ordinary nuclei lying near the stability valley. Such distributions may lead to "pairing of collective degrees of freedom" and, accordingly, to an increase in the interaction cross section, especially in the subbarrier energy region. As was indicated above, an extended distribution of nuclear matter is characteristic of neutron-rich light nuclei, in which the existence of valence neutrons may lead to the formation of a neutron halo. The class of nuclei that have such a structure includes ^{6}He and ^{11}Li. On the other hand, such nuclei are loosely bound, which must lead to an increase in the probability for their breakup, which may be followed by the fusion of the residual nucleus (core) with the target nucleus or by nucleon-transfer reactions not accompanied by the fusion of nuclei. In principle, this wide variety of processes complicates data analysis and entails the need for taking into account all reaction channels. After the first experimental study devoted to exploring fusion–fission reactions that involve ^{6}He nuclei [22], experiments aimed at determining the probability for fusion with ^{6}He nuclei at energies in the vicinity of the Coulomb barrier [24] were performed by using other heavy nuclei. The most recent experiment, performed in Dubna at the DRIBs accelerator complex, confirmed the results concerning the enhancement of the probability for the fusion of nuclei near the Coulomb barrier that feature a neutron halo [25] and interact with $A \sim 200$ nuclei. The cross sections for the formation of compound nuclei were determined versus the projectile energy (excitation function).

Figure 10 shows experimental results obtained by measuring the excitation function for the reaction ^{197}Au(^{6}He, xn)$^{203-xn}$Tl [26, 27]. The cross section and the excitation function for the fusion reaction followed by the emission of two neutrons, whereby a ^{201}Tl nucleus is produced, do not agree with the predictions of the statistical model. The calculated values proved to be much less than the experimental results. The reason may be that the reaction in which the total absorption of a ^{6}He nucleus by a ^{197}Au nucleus occurs has the reaction Q value equal to +12.2 MeV, and this renders the reaction involving the evaporation of two neutrons a deep-subbarrier process. In that case, the calculations of cross sections via a procedure that treats fusion as the penetration of ^{6}He through the barrier may lead to underestimated values. A similar deviation from the results of the calculations based on the statistical model was found in [28] for the excitation function for the reaction ^{206}Pb(^{6}He, $2n$)^{210}Po. On the basis of the results obtained by studying the excitation functions for fusion reactions in the subbarier energy region that are followed by neutron evaporation, we can therefore state that one observes a substantial increase in the cross sections for fusion with ^{6}He nuclei in the vicinity of the Coulomb barrier.

Such an effect can be explained within the two-step fusion model [29, 30]. In this model, one assumes that a sequential transfer of neutrons from a ^{6}He nucleus to the target nucleus occurs. Concurrently, the excitation energy of the nuclear system in question increases by $E_{\text{c.m.}} + Q_{gg}$, which exceeds substantially the Coulomb barrier and leads to the penetration of the alpha particle through the barrier. That the results of the calculations agree with experimental data indicates that the process of sequential neutron transfer for nuclei featuring a neutron halo is likely to be a dominant mechanism affecting the probability for

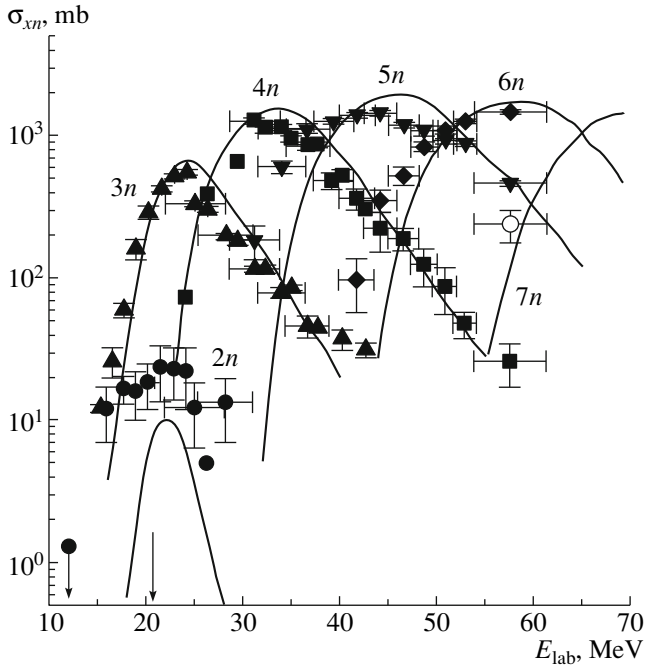

Fig. 10. Excitation functions [27] for the fusion reaction ^{197}Au $+^{6}$ He $\rightarrow^{203-xn}$Tl, where $x = 2$–7. In this figure and in Fig. 11, the solid straight line with an arrow indicates the height of the Coulomb barrier. The solid curves represent the results of the calculations performed on the basis of the statistical model (ALICE-MP code) [28] by using the parameter values of $r_0 = 1.29$ fm, $V = -67$ MeV, and $a = 0.4$ fm.

their fusion and increases the reaction cross section in the deep-subbarrier energy region.

4.3. Nucleon-Transfer Reactions in Loosely Bound Nuclei

An interesting effect was also observed in studying the excitation functions for the reaction of neutron transfer from a ^{6}He nucleus to ^{197}Au target nuclei. Figure 11 gives the excitation functions for the reactions of production of the gold isotopes ^{196}Au and ^{198}Au in the ground state upon ^{6}He interaction with ^{197}Au nuclei. From these data, it follows that the probability for one-neutron transfer leading to the production of ^{198}Au nuclei in this interaction is high ($\sigma \sim 1.2$ b) in the vicinity of the barrier. At the same time, the cross section for the reaction of one-neutron-transfer to the target nucleus decrease smoothly at low energies to the Q_{thr} value, which corresponds to the energy threshold for the reaction.

The cross section for neutron separation from the target nucleus (^{196}Au production) decreases smoothly in the energy region extending to the Coulomb barrier; after that, some saturation of the cross section occurs at a value of 10 mb, whereupon it decreases gradually to the same reaction threshold (Q_{thr}). This may be explained by two mechanisms of ^{196}Au production. Neutron knockout from the target occurs predominantly at energies above the Coulomb barrier. At energies in the vicinity of and below the Coulomb barrier, a leading contribution to ^{196}Au production comes from the evaporation of two neutrons from the ^{198}Au nucleus that can be produced in an excited state near the Coulomb barrier. The cross section for this reaction is commensurate with the total cross section. A large cross section for the transfer of one neutron and a smooth decrease toward the region of low energies (down to 5 MeV) may be due to the mechanism of interaction of a quasifree neutron in the ^{6}He nucleus with the target nucleus.

A similar result is well known for dp reactions, where the cross section grows substantially in the subbarrier energy region (so-called Oppenheimer–Phillips effect) because of the polarization of a loosely bound deuteron. In the case of reactions involving ^{6}He, this effect may be more pronounced because of a lower binding energy of the ^{6}He nucleus in relation to the deuteron and because of stronger Coulomb repulsion forces within the alpha particle of the ^{6}He nucleus in relation to the proton in the deuteron.

The excitation functions for the cross sections for various channels (fusion and nucleon transfer) of ^{6}He-induced reactions versus the difference $E_{\text{c.m.}} - B_c$ are given in Fig. 12 according to data from [30]. Also given here for the sake of comparison is the excitation function for the fusion of ^{197}Au and ^{4}He

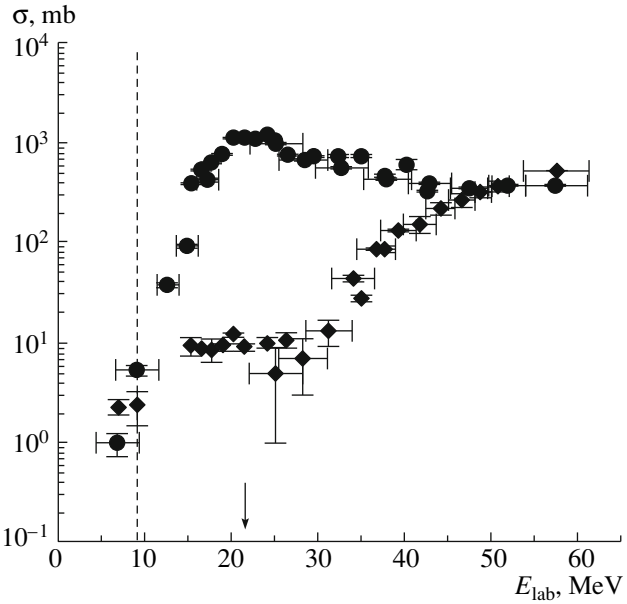

Fig. 11. Excitation function for the ^{197}Au+^{6}He fusion reaction leading to the production of (closed diamonds) ^{196}Au and (closed circles) ^{198}Au nuclei [30]. The vertical dashed straight line indicates the value of Q_{thr}.

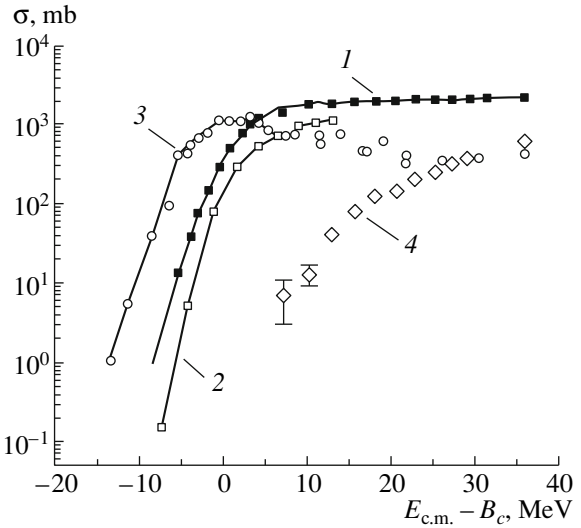

Fig. 12. Excitation functions for the total cross sections for the ^{197}Au+^{6}He (curve *1* and closed boxes represent experimental data from [30]) and ^{197}Au+^{4}He (curve *2* and open boxes represent experimental data from [31]) fusion reactions and reactions of neutron transfer to the target nucleus of ^{198}Au (curve *3* and open circles represent experimental data from [27]) and neutron separation from the target nucleus of ^{196}Au (curve *4* and open diamonds represent experimental data [27]) in a ^{6}He beam. The curves were drawn through the experimental points.

nuclei. One can see an increase in the cross section for ^{197}Au+^{6}He fusion in the subbarier energy region for ^{6}He in relation to its counterpart for ^{4}He and a significant enhancement of the cross section for the reaction where the transfer of one neutron leads to the formation of ^{198}Au.

Thus, the unusual effect of the enhancement of reaction cross sections in the subbarrier energy region for loosely bound nuclei may play an important role for obtaining deeper insight into their structure.

4.4. Manifestation of the Giant Dipole Resonance in Reactions Induced Radiative Nuclear Beams

Experiments with secondary beams made it possible to study the electromagnetic dissociation of exotic

nuclei. The predicted enhanced cross sections for the electromagnetic dissociation of ^{11}Li nuclei were confirmed later [31]. A new type of the collective excitation at low excitation energies was proposed in order to explain an enhanced value of cross sections for Coulomb dissociation. This new excitation mode was called a soft dipole resonance.

In [31], it was assumed that the giant dipole resonance (GDR) may have two components. One of them is an ordinary giant dipole resonance, which is the result of vibrations of all core protons about all core neutrons. The second component, which is precisely the soft dipole resonance, arises as vibrations of the entire core about the halo neutrons.

The amplitude of vibrations that are referred to as the soft mode of the giant dipole resonance depends on the nucleon-density distribution and is proportional to the density-distribution gradient, so that the frequency of its vibrations must be very low. Therefore, the excitation energy of this mode is also expected to be low, in contrast to what we have in the case of an ordinary giant resonance, where the excitation energy is about 20 MeV. Experimental results are indicative of the absence of a collective excitation; moreover, they rule out the assumption of the presence of two halo neutrons in the form of a dineutron. Therefore, a soft dipole resonance should manifest itself in the structure of halo nuclei either as a low-lying dipole level or as a strong enhancement of the reaction cross section in the threshold region upon direct breakup.

An experimental confirmation of the presence of the soft mode of a dipole resonance was obtained for the ^{11}Li nucleus in [32], where the double-charge-exchange pion reaction $^{11}\mathrm{B}(\pi^-,\pi^+)^{11}\mathrm{Li}$ was studied. As a result, a level at $E^* = 1.2 \pm 0.1$ MeV was observed there in the pion spectrum and was assigned a spin–parity of $1/2^+$, $3/2^+$, or $5/2^+$, and it was concluded on this basis that the level in question is excited via an $E1$ transition. In the opinion of the authors of that study, however, this result is not conclusive, since collective states are weakly excited in charge-exchange reactions.

In accord with the results reported in [32], an observation of an excited state of the ^{11}Li nucleus at $E^* = 1.25$ MeV in the $^{11}\mathrm{Li} + p$ reaction was declared in [33], and this was assumed to correspond to the excitation of the halo. In that case, the experimental cross section for inelastic scattering is best described under the assumption of orbital-angular-momentum transfer equal to $L = 1$ (dipole excitation).

Experiments aimed at revealing the existence and nature of a soft dipole mode are being performed at various research centers worldwide (Michigan, USA; RIKEN, Japan; and JINR, Russia).

5. CONCLUSIONS

In the foregoing, we have only dwelt upon part of the problems that are associated with the properties of light nuclei and which are successfully solved with the aid of radioactive nuclear beams. This line of research in nuclear physics is being successfully developed. New-generation accelerator complexes aimed primarily at studying the properties and structure of exotic light nuclei and created at leading research centers worldwide as factories of radioactive beams will provide such beams of intensity up to 10^{11} c^{-1} and will make it possible to perform full-scale experiments with them. In all probability, these new facilities will permit making the next step toward the nucleon drip lines in the region of light nuclei and synthesizing the last light and medium-mass nuclei that are stable against nucleon emission and in which we expect manifestations of new unusual states, structural features, and decay modes.

ACKNOWLEDGMENTS

This work was supported in part by the Russian Foundation for Basic Research (project no. 13-02-00533).

REFERENCES

1. W. T. Diamond, Nucl. Instrum. Methods Phys. Res. A **432**, 471 (1999).
2. Yu. Ts. Oganessian et al., Preprint JINR No. E7-2000-83 (Joint Inst. Nucl. Res., Dubna, 2000).
3. Yu. E. Penionzhkevich, Phys. At. Nucl. **71**, 1127 (2008).
4. N. I. Tarantin, Phys. Part. Nucl. **26**, 440 (1995).
5. L. Gaudefroy, W. Mittig, N. A. Orr, et al., Phys. Rev. Lett. **109**, 202503 (2012).
6. T. Motobayashi et al., Phys. Lett. B **346**, 9 (1995).
7. D. Sohler et al., Phys. Rev. C **66**, 054302 (2002).
8. Yu. S. Lyutostanskii et al., Izv. Akad. Nauk SSSR, Ser. Fiz. **53**, 29 (1989).
9. C. Thibault et al., Phys. Rev. C **12**, 644 (1975).
10. F. Sarazin et al., Phys. Rev. Lett. **84**, 5062 (2000).
11. Yu. E. Penionzhkevich, Phys. At. Nucl **77**, 75 (2014).
12. F. M. Marqués et al., Phys. Lett. B **381**, 407 (1996).
13. I. Tanihata et al., Prog. Part. Nucl. Phys. **35**, 505 (1995).
14. O. M. Knyaz'kov et al., Phys. At. Nucl **59**, 1138 (1996).
15. A. Goldhaber, Phys. Lett. B **53**, 306 (1974).
16. R. Anne et al., Phys. Lett. B **250**, 19 (1990).
17. N. Orr et al., Phys. Rev. Lett. **69**, 2050 (1992).
18. R. Kalpakchieva et al., Phys. At. Nucl. **70**, 619 (2007).
19. K. Arai et al., Phys. Rev. C **51**, 2488 (1995).
20. N. K. Skobelev et al., Z. Phys. A **341**, 315 (1992).
21. Yu. Ts. Oganessian, V. I. Zagrebaev, and J. S. Vaagen, Phys. Rev. Lett. **82**, 4996 (1999).

22. A. S. Fomichev et al., Z. Phys. A **351**, 129 (1995).
23. M. S. Hussein et al., Phys. Rev. C **46**, 377 (1992).
24. J. J. Kolata et al., Phys. Rev. Lett. **81**, 4580 (1998).
25. A. Lemasson et al., Phys. Rev. Lett. **103**, 232701 (2009).
26. Yu. E. Penionzhkevich, Int. J. Mod. Phys. E **20**, 938 (2011).
27. N. K. Skobelev, Phys. At. Nucl. **77** (11) (2014, in press).
28. Yu. A. Muzychka and B. I. Pustylnik, in *Proceedings of the International School–Seminar on Heavy-Ion Physics, Alushta, 1983,* Preprint JINR No. D7-83-644 (Joint Inst. Nucl. Res., Dubna, 1983), p. 420.
29. V. I. Zagrebaev, Phys. Rev. C **67**, 061601(R) (2003).
30. Yu. E. Penionzhkevich et al., Phys. Rev. Lett. **96**, 162701 (2006).
31. S. M. Lukyanov et al., Phys. Lett. B **670**, 321 (2009).
32. T. Kobayashi et al., Nucl. Phys. A **538**, 343 (1992).
33. A. A. Korsheninnikov et al., Phys. Rev. C **53**, R537 (1996).